Applied Catalysis B: Environmental 224 (2018) 295–304

Contents lists available at ScienceDirect

Applied Catalysis B: Environmental

journal homepage: www.elsevier.com/locate/apcatb

A study on the deactivation and reactivation of a Ni/Al_2O_3 aldehyde hydrogenation catalyst: Effects of regeneration on the activity and properties of the catalyst

Sinqobile V.L. Mahlaba, Jignesh Valand, Abdul S. Mahomed, Holger B. Friedrich*

Catalysis Research Group, School of Chemistry and Physics, University of KwaZulu-Natal, Private Bag X54001, Durban, 4000, South Africa

ARTICLE INFO

Keywords:
Deactivation
Phosphorus
Phosphine
Hydrogenation
Nickel

ABSTRACT

The effectiveness of different experiments for the regeneration of a phosphorus poisoned 15 wt.% Ni/Al_2O_3 catalyst was investigated during the time on stream hydrogenation of octanal to octanol. The catalyst was deactivated after being exposed to feed contaminated with 500 ppm of triphenylphosphine. Regeneration of the catalyst was attempted by either treating the poisoned catalyst with hydrogen, washing the catalyst with octanol or conducting a combined octanol wash-hydrogen treatment experiment, all at elevated temperatures and at atmospheric pressure. The combined regeneration experiment was the most effective, since the conversion and octanol selectivity were recovered to a significant extent. Characterisation of the regenerated catalysts by ICP-OES, XRD, magnetic measurements and TEM showed that sintering also contributed to the deactivation of the catalysts, and that regeneration did not remove phosphorus from the catalyst, due to phosphorus having reacted with nickel. It was also established that some phosphorus was incorporated into the alumina support to generate strongly acidic sites.

1. Introduction

One of the most common industrial homogeneously catalysed reactions is the hydroformylation of olefins in the presence of synthesis gas to yield aldehydes [1]. This process is usually catalysed by a homogeneous rhodium catalyst containing phosphine or phosphite ligands, and is an intermediate step in the production of primary alcohols [2,3]. The resultant alcohols are used in a number of industrial and synthetic applications such as the manufacture of detergents, fine chemicals and pharmaceuticals, cosmetics, as solvents, and polymer plasticisers [1,4–9].

Aldehydes are typically hydrogenated to their corresponding alcohols over transition metal catalysts supported on high surface area oxides. Metals that have been used traditionally include those belonging to the platinum group of metals (PGMs) such as Pt, Pd, Ru and Rh, while the use of Ni, Cu and Co later became more commonplace [4,5,8,10,11]. Nickel is preferred since it is much cheaper, and more abundant, compared to the PGMs. It's high activity and relatively lower cost has led to it finding applications in a wide variety of industrial catalytic processes such as hydrogenation, hydrodesulphurization, methane reforming and CO methanation [12–15].

An important consideration in any catalytic process is the long-term stability of the catalyst. Deactivation of catalysts presents significant problems, such as the generation of large volumes of wastes, loss of production due to process shutdowns, and further environmental costs associated with treatment and disposal of the deactivated catalyst [16,17]. The options that exist for deactivated catalysts are either disposal or regeneration. The former is undesirable from an economic and environmental standpoint, since it results in the loss of expensive metals, while environmental laws regulating the disposal of potentially harmful materials have become more stringent. Hence, disposal is considered the last resort. A more desirable alternative is regeneration, which is the treatment of the catalyst with the aim of recovery and/or restoration of lost catalytic activity [18].

Hence, understanding how deactivation occurs and how to perhaps reverse its effects, is a crucial aspect to address. When considering the tandem process of hydroformylation and hydrogenation, an important factor is the possible transfer of phosphorus based ligands to the hydrogenation reactor. Phosphorus is a known poison which deactivates metallic catalysts used in hydrogenation, methanol synthesis and automotive catalysts [19–22], and is, thus, a potential poison for nickel based aldehyde hydrogenation catalysts, since it is known to have a high affinity to nickel [23,24].

The regeneration of sulphur poisoned hydrogenation catalysts has

* Corresponding author.
E-mail addresses: friedric@ukzn.ac.za, holgerbfriedrich@gmail.com (H.B. Friedrich).

http://dx.doi.org/10.1016/j.apcatb.2017.10.064
Received 28 July 2017; Received in revised form 16 October 2017; Accepted 26 October 2017
Available online 28 October 2017
0926-3373/

been extensively studied, with most involving treatment of the poisoned catalyst with hydrogen at elevated temperatures to remove the adsorbed sulphur [25–27]. The regeneration of phosphorus poisoned hydrogenation catalysts, however, has received very little attention. A patent by Kim *et al.* [28] reports a regeneration procedure of a Ni catalyst poisoned with a phosphine compound. The catalyst was seemingly successfully regenerated using hydrogen at elevated temperatures, although it was not stated to what extent.

Considering how little has been published addressing the detrimental effects of phosphorus on hydrogenation catalysts, or the possible regeneration treatments of such catalysts, a study of the effects of phosphorus poisoning on the activity and selectivity of nickel hydrogenation catalysts supported on γ-Al_2O_3 was undertaken in this body of work. In addition to understanding the interaction of the poison with the catalyst, we looked at regeneration protocols and their effectiveness for the removal of the adsorbed poison, and subsequent levels of recovery of the catalytic activity. We see application of this methodology in plants and processes using hydrogenation technology with Ni catalysts that may be susceptible to phosphorus poisoning.

2. Experimental procedure

2.1. Catalyst synthesis

Nickel (15 wt.%) was deposited on high surface area γ-Al_2O_3 (Alpha Aeser) using the wet impregnation method [29]. An appropriate mass of nickel nitrate hexahydrate ($Ni(NO_3)_2 \cdot 6H_2O$, Sigma-Aldrich, Cas No: 13478-00-7, P-Code 33209101) was dissolved in deionised water and added to the support slurry. The mixture was stirred for three hours at room temperature, ultra-sonicated for half an hour at room temperature, and subsequently stirred for an additional hour [30–32]. The excess solvent was evaporated by heating, and the remaining paste was dried overnight in an oven at 110 °C. The resultant solid was ground and calcined for five hours under a stream of air at 550 °C [14]. Prior to hydrogenation reactions, the calcined precursor was pelletised and crushed to particles sized between 300 and 600 μm [29]. All subsequent experiments were performed using the same batch of catalyst.

2.2. Fresh and used catalyst characterisation

The surface area of the calcined and used catalysts was determined by the BET method, using nitrogen physisorption with a six port Micromeritics ASAP 2420 instrument. The samples were degassed under vacuum at 250 °C, cooled, weighed, then analysed at −196 °C.

The nickel loading and phosphorus content of the catalysts were quantified using inductively coupled plasma-optical emission spectroscopy with a Perkin Elmer Precisely Optima DV 5300 Optical emission spectrometer. Prior to analysis, the samples were digested using aqua regia (1:3 nitric acid to hydrochloric acid) on a CEM Mars 6 OneTouch Technology microwave digestion unit, using easy prep sample vessels at a maximum temperature of 200 °C and pressure of 328 psi.

The crystalline phases of the prepared catalyst were identified by powder x-ray diffraction using a Bruker Advance D8 diffractometer equipped with an Anton Paar XRK 900 reaction chamber and TCU 750 temperature control unit. The instrument employed a Cu K_α radiation source with a wavelength of 1.5406 Å [33].

The metal dispersion of nickel on the alumina support was measured by hydrogen chemisorption on a Micromeritics ASAP 2020 Surface Area and Porosity analyser. The catalyst was first reduced by heating it at a rate of 10 °C min^{-1} under a flow of pure hydrogen to 550 °C. After reduction at this temperature for 240 min, the catalyst was cooled to 35 °C, the temperature at which the chemisorption analysis was conducted. After chemisorption, the temperature was increased to 550 °C. Oxygen titration was then performed at this temperature to determine the degree of reduction.

Transmission electron imaging was performed using a Joel JEM 1010 Electron Microscope equipped with iTEM software for image capture and analysis.

The magnetic properties of the fresh, poisoned and regenerated catalysts were measured on a Lakeshore Model 735 vibrating sample magnetometer. The measurements were taken at room temperature. A mass of 20 mg of sample was loaded onto the sample holder, attached to the sample rod and placed inside a Janis model helium cryostat. Measurements were conducted in an applied external magnetic field range within −14 to 14 kOe.

Infrared spectra of the fresh and used catalyst samples were obtained using a Perkin Elmer FTIR Spectrometer RX using a KBr disc. Approximately 3 mg of sample was ground in a mortar and pestle with approximately 300 mg of KBr, then compressed into a disc which was analysed by the FTIR spectrometer.

Cross sectional scanning electron microscopy imaging was performed on the fresh and used catalyst samples. The samples were mixed with Akasel epoxy resin and Akasel cure in plastic moulds, then cured for 24 h to form resin blocks. The blocks were then polished using diamond paste to obtain a smooth surface, then coated with carbon to prevent charging. The back scattered electron imaging and electron dispersive X-ray spectroscopy analysis were carried out on a Zeiss EVO 40 instrument with a tungsten filament, at an accelerating voltage of 20 kV, a probe current of 1.5 nA and a filament current of 2.403 A. EDS analyses were performed using a Bruker XFlash SDD detector, controlled by Bruker Esprit software.

Pulse chemisorption-TPD-MS experiments were carried out on an AutoChem 2920 (Micromeritics, USA) instrument coupled with a Cirrus Mass Spectrometer (MKS Instruments) to quantify the Brønsted acid sites on the fresh and regenerated catalyst samples. Each sample (50 mg) was placed in a quartz U-tube between layers of glass wool. The samples were first heated to 550 °C at a rate of 10 °C min^{-1} under a flow of helium (99.99%, Afrox). The samples were then cooled to 100 °C for pulse chemisorption, where 15 cm^3 of *n*-propylamine vapour were dosed in 1 cm^3 pulses. The Brønsted acid sites were quantified by carrying out the temperature programmed desorption from 100 to 550 °C at a heating rate of 10 °C min^{-1} and mass spectrometry was used to distinguish between the desorbing species (propylamine, propene and ammonia). The amount of desorbed propene was then used to quantify the Brønsted acid sites.

2.3. Catalytic testing and time on stream regeneration

Accelerated time on stream deactivation and regeneration experiments were performed in a stainless steel, continuous flow fixed bed reactor. A volume of 2 mL (1.44 g) of catalyst was diluted with 2 mL of 24 grit carborundum and placed between two layers of glass wool at the reactor hot zone, while the rest of the tube was packed with carborundum. The hydrogenation of octanal (Plant feed, 83% purity) diluted in octanol (Plant feed, 92% purity) was performed at 140 °C, at a liquid hourly space velocity of 18 h^{-1} and a pressure of 50 bar. The substrate to hydrogen ratio was set at 1:2, and the reaction products were quantified using a GC-FID by injection into a Perkin Elmer Precisely Clarus 500 gas chromatograph (BP1-PONA column) to establish and monitor the conversion and selectivity of the catalyst. The different by-products were identified by injecting the C_{16} diol and C_{24} acetal standards (99.99% purity, Sigma Aldrich). Previous studies have shown that the use of octanol as a solvent does not affect the reaction equilibrium, and, hence, has no adverse effects on the hydrogenation of octanal to octanol [34].

Prior to reactions, the catalyst underwent in situ reduction under a stream of hydrogen (Afrox, 99.99% purity) diluted in nitrogen (Afrox, 99.99% purity). The hydrogen concentration was increased over a period of time in the presence of nitrogen, until a concentration of 100% was reached, at 350 °C. The temperature was then increased to 450 °C, the temperature at which the catalyst was reduced for a period of 8 h, then cooled to 140 °C. Time on stream testing of the catalyst,

including poisoning and regeneration, was performed in five steps. The first step was the hydrogenation of feed consisting of 10 wt.% octanal in octanol (termed clean feed, **CF**) to evaluate the intrinsic activity of the catalyst towards the hydrogenation of octanal. The clean feed was hydrogenated until stable conversion and selectivity was achieved. The poisoned feed, consisting of 500 ppm of triphenyl phosphine (99% purity, Sigma-Aldrich) used to simulate the ligand from a hydroformylation catalyst, was subsequently introduced, until the catalytic activity had sufficiently declined (an accelerated poisoning procedure). This was established by monitoring the decline of the conversion of octanal by GC-FID. After the conversion had declined to about 30%, the flow of the poisoned feed was stopped, and the clean feed was reintroduced to gauge the extent of deactivation prior to regeneration. Thereafter, regeneration experiments were carried out, and the catalytic activity was re-evaluated for the conversion of octanal and selectivity to octanol by the introduction of clean feed. Three different regeneration procedures were attempted, namely, a hydrogen treatment, octanol washing procedure and a combination of the two.

The regeneration experiments were performed following the procedure described. This included regeneration with hydrogen (20 mL min^{-1}), regeneration by washing with octanol (at a flow rate of 0.6 mL min^{-1}), and a regeneration experiment that involved washing the catalyst bed with octanol, followed by a hydrogen treatment, which was termed the combined regeneration procedure. The hydrogen treatment and solvent wash regeneration experiments were each conducted for about 20 h, while the combined regeneration was conducted for approximately 24 h (12 h octanol wash, followed by 12 h of hydrogen treatment). For each of the regeneration experiments, the reactor pressure was slowly decreased to atmospheric pressure and the temperature was increased to 200 °C. After each regeneration step was carried out, the reactor was cooled to 140 °C, re-pressurised to 50 bar, and the reaction was restarted by introducing clean feed.

3. Results

3.1. Fresh catalyst characterisation

3.1.1. Physico-chemical characteristics

Table 1 presents the textural and physico-chemical properties of the support and the calcined Ni catalyst. The deposition of metal resulted in a decrease in surface area, pore volume and pore size of the support, indicative of pore occupation by the supported metal. The nickel loading was 14.5 wt.%, which is close to that of the desired value. According to results from the chemisorption analysis, nickel was dispersed as small crystallites on the support.

3.1.2. Powder X-ray diffraction

Fig. 1 shows the X-ray diffractograms of the calcined 15 wt.% nickel on alumina catalyst as well as the alumina support. The XRD pattern shows peaks corresponding to the alumina support, as well as to the bunsenite NiO phase (JCPDS No. 78-0643) [35]. The broadness of the peaks is due to the amorphous nature of alumina, as well as the formation of well dispersed, small NiO crystallites on the support. The diffractogram is similar to that obtained by Yenumala et al. [36] for a 15 wt.% alumina supported catalyst.

3.1.3. Transmission electron microscopy

Fig. 2 shows the TEM image of the 15 NiA catalyst, along with the particle size distribution histogram. The NiO particles appear darker and have a spherical morphology, while the lighter, needle shaped particles are those of the support [37]. The average size of the NiO particles was 7 nm, with most of them falling within a range of 3–12 nm, while a small fraction of particles fall outside this range.

3.2. Time on stream catalyst activity

3.2.1. Deactivation of 15 NiA

Fig. 3 shows the catalytic activity during the hydrogenation of clean feed (**Zone A**), during the hydrogenation of TPP contaminated feed (**Zone B**) and after the reintroduction of clean feed (**Zone C**). The steady state conversion and octanol selectivity, shown in **Zone A**, were 98% and 88% respectively prior to the introduction of poisoned feed. The sum of the selectivity toward by-products, which included C_{24} acetal and aldol condensation products, formed on acid sites on the support, was 10% [34,38]. The introduction of the poisoned feed (**Zone B**) resulted in a sharp decline in octanal conversion, while the selectivity remained relatively constant during the poisoning run. This suggests non-selective adsorption of the phosphine ligand on both the Ni metallic sites and the acid sites of the support, resulting in an overall decrease in activity. When the clean feed was reintroduced (**Zone** C), the conversion reached a steady state value of 20% with no further deactivation. The octanol selectivity decreased to about 50%, whilst that of the C_{24} acetal increased to 40%.

The decrease in conversion after the introduction of the poisoned feed was due to the adsorption of phosphorus on both the active metallic sites and the support, as observed previously in other work [39,40]. Phosphorus is a strong electron donor and chemisorbs onto the vacant d-orbital of the metal via its lone pair of electrons [41]. The π back-donation of the metal into a phosphorus 3d orbital further strengthens the bond between metal and phosphorus, making it highly covalent. This renders the removal of phosphorus difficult under reaction conditions, leading to its accumulation on the catalyst surface [23,42]. Phosphorus also reacts with nickel to form an amorphous nickel-phosphorus layer (Ni_xP_y) on the nickel active sites. This layer has little activity, thus also preventing recovery of the catalyst in aldehyde hydrogenation when the poisoned feed was removed [43].

The C_{24} acetal selectivity increased markedly when the clean feed was reintroduced (**Zone C**), whilst a subsequent decrease in octanol selectivity was observed. This behaviour suggests an increase in the acidity of the catalyst, indicated by the higher rate of acetal formation. The higher acidity is ascribed to the formation of $AlPO_4$ sites from the reaction of water, phosphorus and alumina. Water forms as a by-product due to reactions catalysed by the support, such as the formation of the C_{16} diol by aldol condensation, C_{24} acetal and dioctyl ether. The water creates an oxidising environment that oxidises phosphorus species, thereby allowing their reaction with alumina to form $AlPO_4$ [44,45]. The interaction of TPP with the catalyst surface and the formation of both Ni_xP_y and $AlPO_4$ is shown in Scheme 1.

3.2.2. Regeneration by H_2

The first attempt at regeneration involved passing hydrogen over the poisoned catalyst at a fixed temperature of 200 °C, at atmospheric pressure. Thus, after poisoning and reinstating clean feed for ten hours, the feed was stopped and hydrogen was passed over the catalyst at atmospheric pressure for about 20 h. The activity profile after hydrogen regeneration is presented in Fig. 4. **Zone C** is the duplication of the step

Table 1
Physico-chemical properties of the support and 15 wt.% nickel catalyst.

Sample	Ni elemental composition (wt.%)	BET area (m^2g^{-1})	Pore volume ($cm^3\ g^{-1}$)	Metal dispersion (%)	Ni surface area ($m^2\ g^{-1}$)	Crystallite size (nm)
γ-Al_2O_3	–	232	0.8	–	–	–
15 Ni/Al_2O_3	14.5	176	0.5	10.3	9.9	9.9

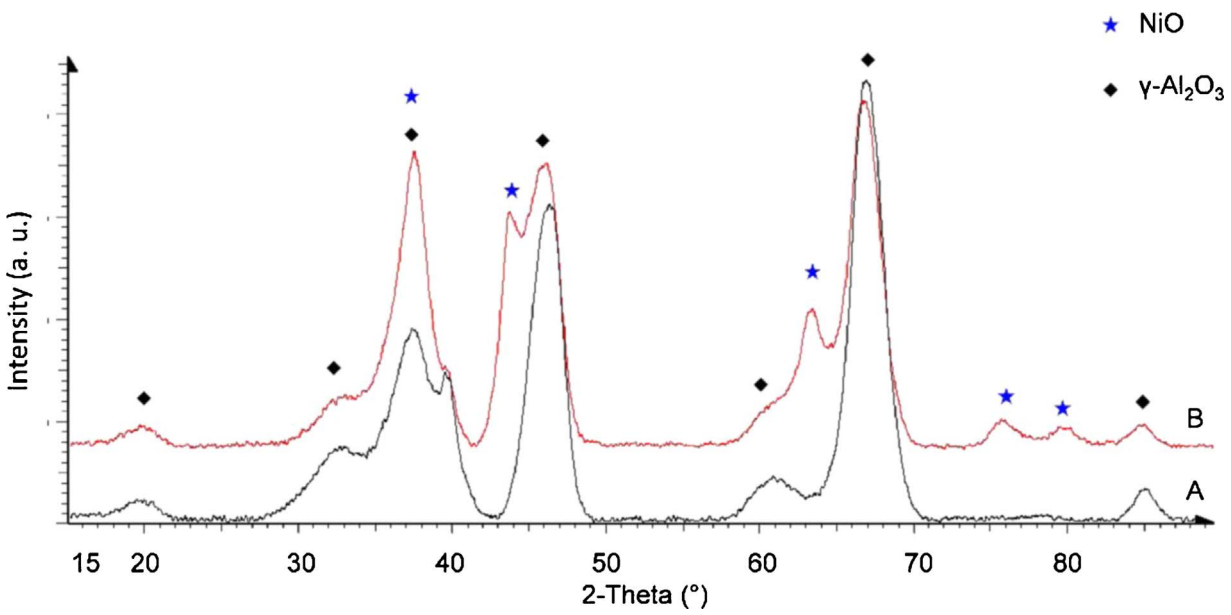

Fig. 1. XRD pattern of (A) the alumina support and (B) 15 wt.% nickel on γ-Al_2O_3.

from Fig. 3 to show continuity, **Zone D** represents the time passing during the regeneration step and **Zone E_I** shows the activity after re-introducing the clean feed. After regenerating the catalyst for 20 h and reintroducing the clean feed, a steady state conversion of about 50% was attained. However, as observed prior to regeneration, the acetal selectivity increased further and did not reach steady state. The higher C_{24} acetal selectivity indicates a significant increase in acidity of the catalyst.

We surmise that treatment of the catalyst with hydrogen at high temperatures during the regeneration step, induced the diffusion of phosphorus into the nickel particles, forming metastable Ni-P phases, as shown in Scheme 2. The phosphidation of Ni supported catalysts with TPP has been reported before, however, with catalysts containing much more nickel [46,47]. The authors show that the incorporation of phosphorus into the catalyst, under reducing conditions, occurs easily at a temperature of about 170 °C to form Ni_2P, lower than the regeneration temperature reported here.

It would follow from this argument that during the reintroduction of clean feed and at the lower reaction temperature, the phosphorus from the metastable Ni_xP_y particles could possibly diffuse out and dope the surface of the cleaned nickel surface atoms, and redistribute on the alumina. This would result in the formation of more acidic sites, in this case $AlPO_4$, from the reaction of the alumina support with oxidised phosphorus species. The presence of the $AlPO_4$ phase was confirmed by FTIR as shown in the supplementary information (Figs. S1 to S5).

This spill-over of phosphorus may also form acidic P-OH groups that result from the hydroxylation, protonation or hydration of surface P atoms by water [44,45,49,50], thus leading to the continuous increase in acetal selectivity and subsequent decline in octanol selectivity, as observed in Fig. 4, **Zone E_I**. Li *et al.* [51] showed that doping of a γ-alumina supported nickel catalyst with triphenylphosphine resulted in an increase in the total number of acid sites of the material. This was also seen by Buwono *et al.* [40] and Sawhill et al. [52], who reported on the formation of an $AlPO_4$ layer close to the supported metal particles or sometimes at the interface of the metal and support, when the alumina supported catalysts were exposed to phosphine species. This led us to infer that alumina acts as a poison reservoir, while hydrogen only cleans some nickel sites, and fails to remove poison adsorbed on the support.

3.2.3. Regeneration by octanol washing (OW)

Next, a method involving the use of a solvent, in this case octanol, as a 'washing' agent to remove the poison was investigated. Fig. 5 presents the activity profile of 15 NiA after the solvent wash regeneration. When

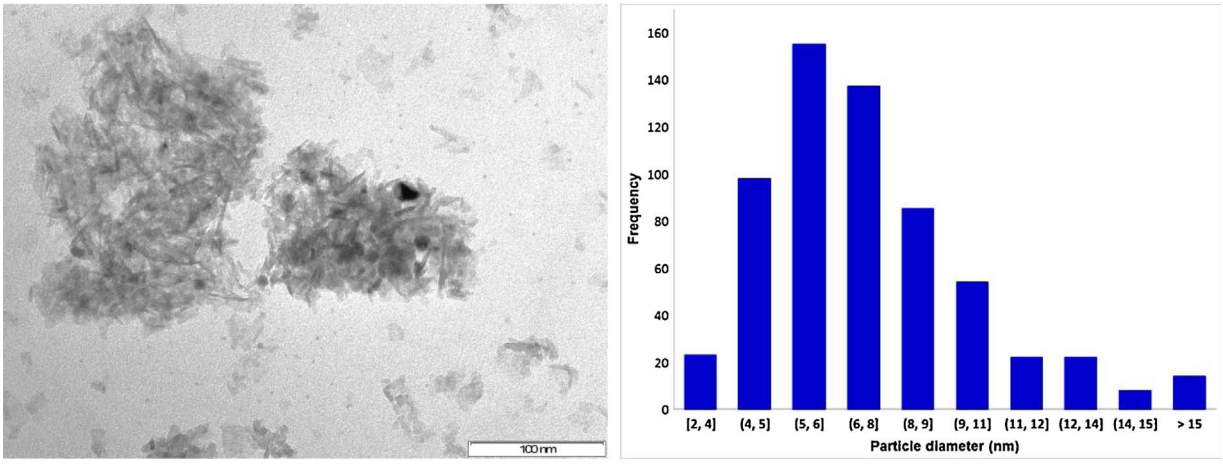

Fig. 2. TEM image of 15 wt.% Ni on alumina and the NiO particle size distribution histogram.

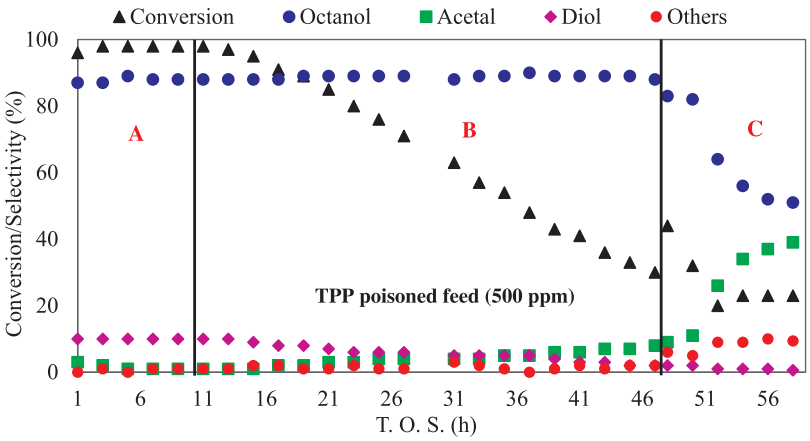

Fig. 3. Activity profile of the 15 NiA catalyst before, during and after exposure to poisoned feed: (**A**) clean feed, (**B**) TPP feed, (**C**) clean feed.

comparing the results presented in Fig. 5 to those in Fig. 4, several differences are evident. The octanol selectivity was observed to be higher after washing the poisoned catalyst with octanol than after the hydrogen treatment procedure, while the recovery in activity was also comparatively higher. It can also be observed from Fig. 5 that the selectivity was much more stable for the two major products (octanol and the acetal) after this regeneration step.

From the results in Fig. 5, we conclude that the conditions favoured dissolution of weakly adsorbed phosphorus from some nickel sites, while the relatively high regeneration temperature induced the diffusion of phosphorus into the nickel, but to a minor extent. Chakrabarti *et al.* [53] conducted a study on the regeneration of Rh catalysts poisoned by inorganics such as Na, S and P. Although it is not explicitly explained, the authors claim the re-introduction of clean feed led to a slight reversal of the poisoning effects of phosphorus [53].

3.2.4. Combined regeneration (SH)–solvent washing and hydrogen

The third regeneration experiment involved a combination of the two previous experiments, and involved an octanol washing step for approximately 12 h, followed by passing hydrogen over the catalyst for a further 12 h. The activity profile of the catalyst after this regeneration procedure (Fig. 6) shows a significant recovery of the activity, while the selectivity towards octanol was also significantly higher than after either of the individual regeneration procedures.

The solvent likely serves to wash off weakly bound phosphorus species on the support, as well as to dissolve and remove soluble Ni-P complexes on nickel sites, while hydrogen serves to clean some of the Ni centres by inducing the diffusion of phosphorus into the nickel bulk. This resulted in improved recovery of catalytic activity compared to the previous regeneration procedures.

3.3. Used catalyst characterisation

3.3.1. Physico-chemical properties

The results presented in Table 2 show a decrease in the BET surface area of the poisoned and regenerated catalysts, which is indicative of deposition of carbonaceous species on the alumina support, but could also indicate agglomeration of nickel. The nickel loading on the used catalysts remains fairly constant, suggesting stability of the catalyst against leaching. The elemental analyses also confirmed the retention of phosphorus by the catalysts, despite regeneration. The phosphorus content is not significantly different for all the catalysts, suggesting that regeneration was unable to remove phosphorus from the catalyst bed, but merely redistributes it. The manner of redistribution is dependent on the regeneration procedure.

3.3.2. XRD and magnetism

As shown in Fig. 7, there are no distinguishable peaks that can be attributed to the formation of a distinct nickel phosphide phase on the poisoned catalysts. In addition, the peaks for Ni appear extremely broad for the 15 NiA-P catalyst, which suggests that some nickel has remained unaffected by the phosphorus and hence present themselves as well dispersed particles. We thus surmise that much of the nickel has reacted with phosphorus to form a largely amorphous nickel phosphide phase on the catalyst, as similarly reported by Tan et al. [47]. The absence of peaks attributable to distinct nickel phosphide phases on the poisoned catalysts suggests that the reaction between nickel and phosphorus results in the formation of small, well dispersed particles on the support. Alternatively, the nickel phosphide phase that may form is possibly non-crystalline, since the regeneration temperature is below 300 °C. According to Tan et al. [47], crystallization of nickel phosphide occurs at about 300 °C. We also performed high temperature in situ

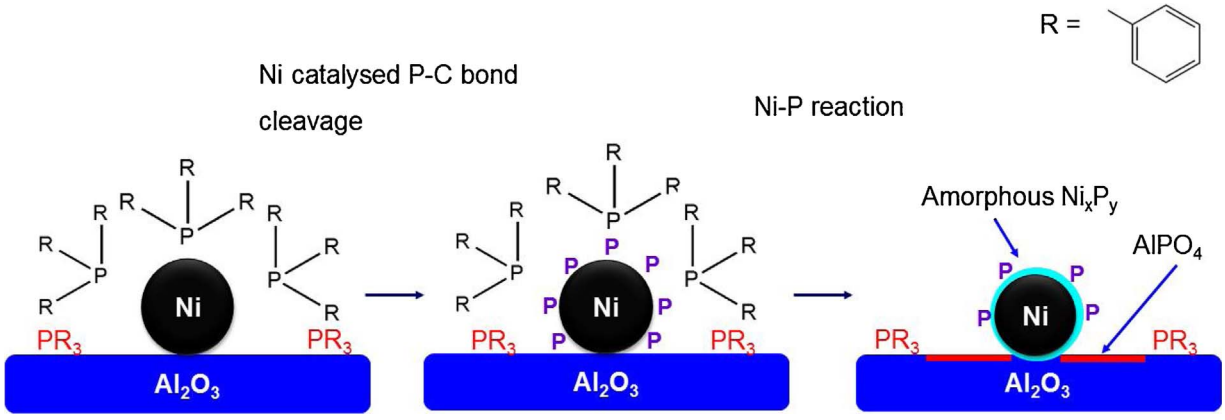

Scheme 1. Adsorption and reaction of triphenylphosphine with nickel particles and the support.

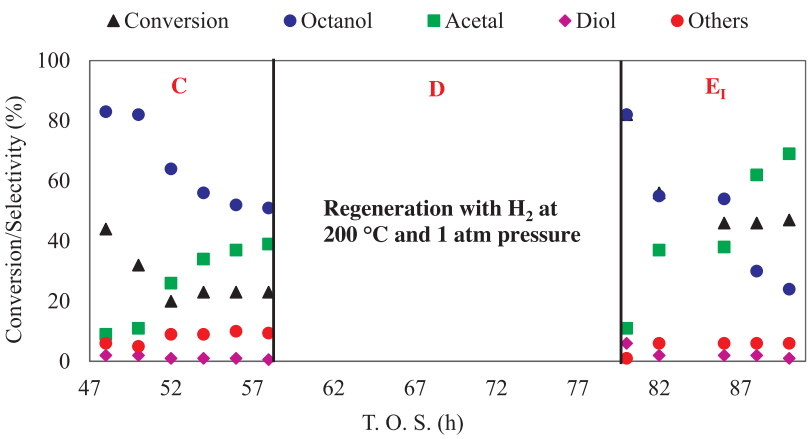

Fig. 4. Activity profile of 15 NiA before and after regeneration with hydrogen: (**C**) clean feed before regeneration, (**D**) regeneration step, ($\mathbf{E_I}$) clean feed after regeneration.

XRD to establish the formation of the nickel phosphides phases, but this proved unsuccessful, likely due to the well dispersed nature of these crystallites.

Magnetic measurements, however, showed that phosphorus did react with nickel, since there was a decrease in the magnetic character of the poisoned catalyst samples, indicated by their lower saturation magnetization value, as seen from the magnetic hysteresis loops in Fig. 8. Metallic nickel is ferromagnetic, whereas doping nickel with phosphorus has been shown to induce a change in the magnetic character, making nickel paramagnetic [54]. This was seen by results in Fig. 8, where the saturation magnetization of reduced 15 NiA was higher, with a value of 4.0 emu/g, while those of the poisoned catalysts were much lower. The saturation magnetization values of 15 NiA-P, 15 NiA-H, 15NiA-S and 15 NiA-SH samples were measured to be 0.9, 1.3, 0.9 and 1.3 emu/g respectively (see Table 2 for coding).

The lower saturation magnetization of the poisoned and regenerated catalysts indicates an interaction between Ni and P. This means the catalysts lose their ferromagnetism, and become paramagnetic after reacting with phosphorus, a property that has been observed during the synthesis of nickel phosphide nanoparticles from a reaction of nickel nanoparticles with trioctylphosphine as a phosphorus source [43,54,55]. However, the materials do not lose their ferromagnetism entirely, indicating that not all nickel reacts with phosphorus [54].

3.3.3. Transmission electron microscopy

Transmission electron microscopy imaging of the fresh, used, poisoned and regenerated catalysts was carried out to observe the changes in the size, morphology and distribution of the nickel particles on the support (Fig. 9). In addition to these images, the average particle size associated with each of these materials is given in Table 2.

As shown in Fig. 9, it can be observed that the Ni particles have sintered to a significant extent when compared to the fresh (Fig. 9A) and non-poisoned, used catalyst (Fig. 9B). This sintering is ascribed to phosphorus induced migration of the Ni particles to form these larger clusters. This phenomenon has been reported previously, albeit for different investigations [56]. The clustering of the Ni particles was more prominent for the poisoned (Fig. 9C), hydrogen regenerated (Fig. 9D) and the solvent washed (Fig. 9E) catalysts.

As a consequence of this behaviour, the Ni surface area was further lowered, leading to the decrease of the overall activity, as well as the selectivity to octanol. The TEM image of the 15 NiA-SH catalyst (Fig. 9F) also showed some clustering, however, it was noticed that it was to a lesser degree than the other regenerated catalysts. The effect of this was a catalyst that yielded more octanol than those obtained after the other regeneration experiments. This conclusion was supported by the quantity of hydrogen uptake by the fresh and regenerated catalysts, obtained from the temperature programmed desorption of hydrogen. From Table S1, it was observed that the hydrogen uptake of the fresh 15 NiA catalyst was higher than that of the regenerated catalysts (15 NiA-H and 15 NiA-SH).

3.3.4. Acidity measurements

The *n*-propylamine TPD profiles of the 15 NiA, 15 NiA-H and 15 NiA-SH catalysts are presented in Fig. S7, and the number of acid sites per material, based on the amounts of evolved propylene, from the decomposition of adsorbed *n*-propylamine, are presented in Table 2. The regenerated catalysts presented a higher density of acid sites compared to the fresh, reduced 15 NiA catalyst, which is attributed to the formation of the $AlPO_4$ phase on the support [52,57].

Phosphorus has been reported to interact with the alumina support to form an acidic $AlPO_4$ phase [40,57,58], and the increase in the C_{24}

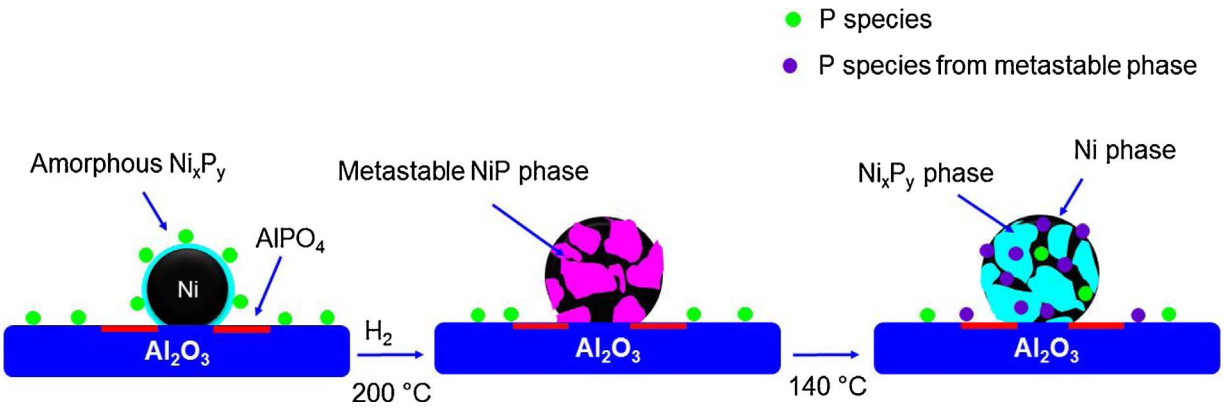

Scheme 2. Simplified model of the temperature induced formation of metastable Ni_xP_y and subsequent diffusion of P from the metastable phase to re-poison nickel active sites under process conditions [47,48].

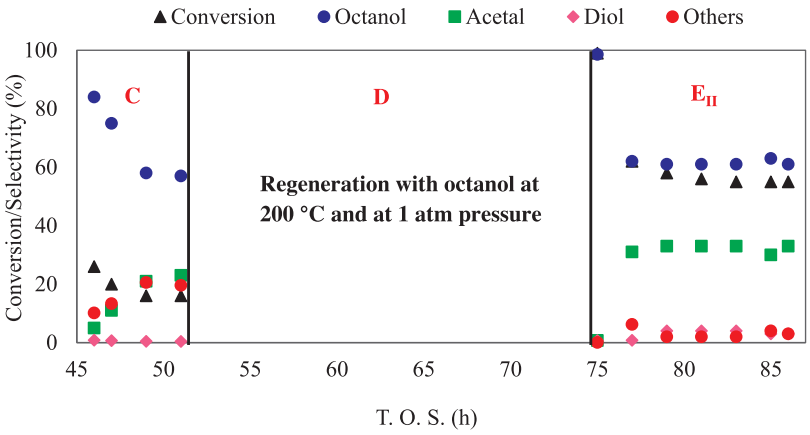

Fig. 5. Activity profile of 15 NiA before and after regeneration with octanol: **(C)** clean feed before regeneration, **(D)** regeneration step, **(E_{II})** clean feed after regeneration.

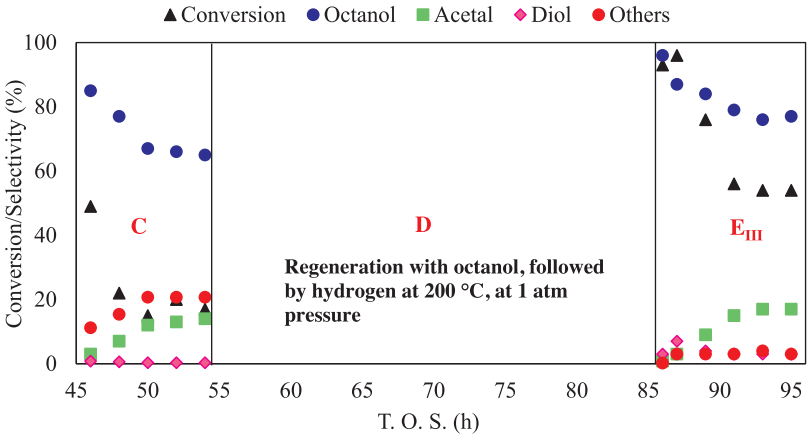

Fig. 6. Activity profile of 15 NiA before and after regeneration with octanol and hydrogen: **(C)** clean feed before regeneration, **(D)** regeneration step, **(E_{III})** clean feed after regeneration.

Table 2
Textural properties and elemental composition (Ni and P) of fresh and used catalysts.

Sample name	Ni (wt.%)	P (wt.%)	BET surface area (m^2/g)	Pore volume (cm^3/g)	Average particle size
NiA–fresh catalyst	14.5	0	176	0.52	7
15-NiA-U–used, non-poisoned	14.5	0	138	0.31	8
15-NiA-P–poisoned with TPP	14.6	1.6	143	0.29	17
15-NiA-H–regenerated with H_2	14.2	1.5	126	0.29	19
15-NiA-S–regenerated with octanol	14.6	1.8	133	0.29	22
15-NiA-SH–regenerated with octanol and H_2	15.0	1.7	130	0.29	13

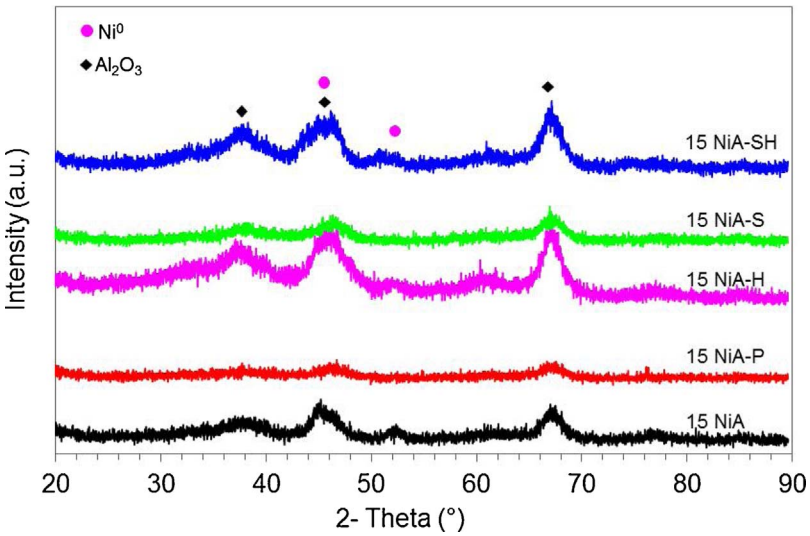

Fig. 7. Powder X-ray diffraction patterns of the reduced, poisoned, and regenerated 15 NiA catalysts.

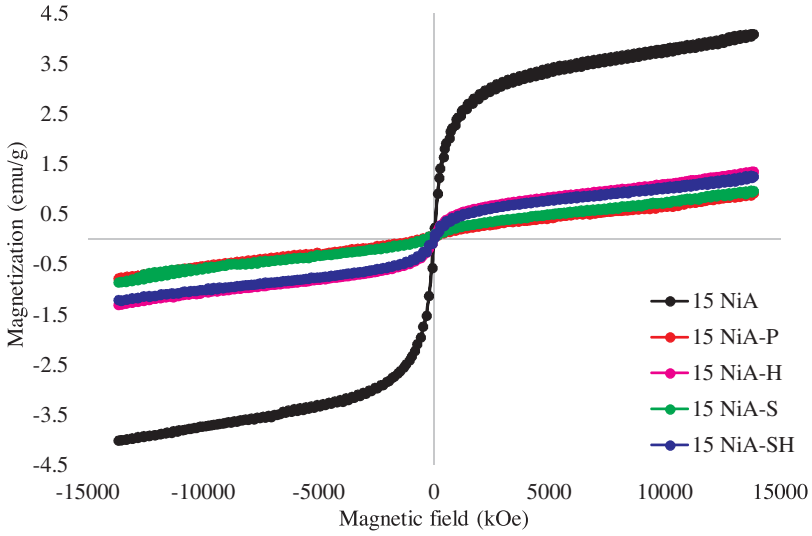

Fig. 8. Magnetic hysteresis loops for 15 NiA, 15 NiA-P, 15 NiA-H, 15 NiA-S and 15 NiA-SH at room temperature.

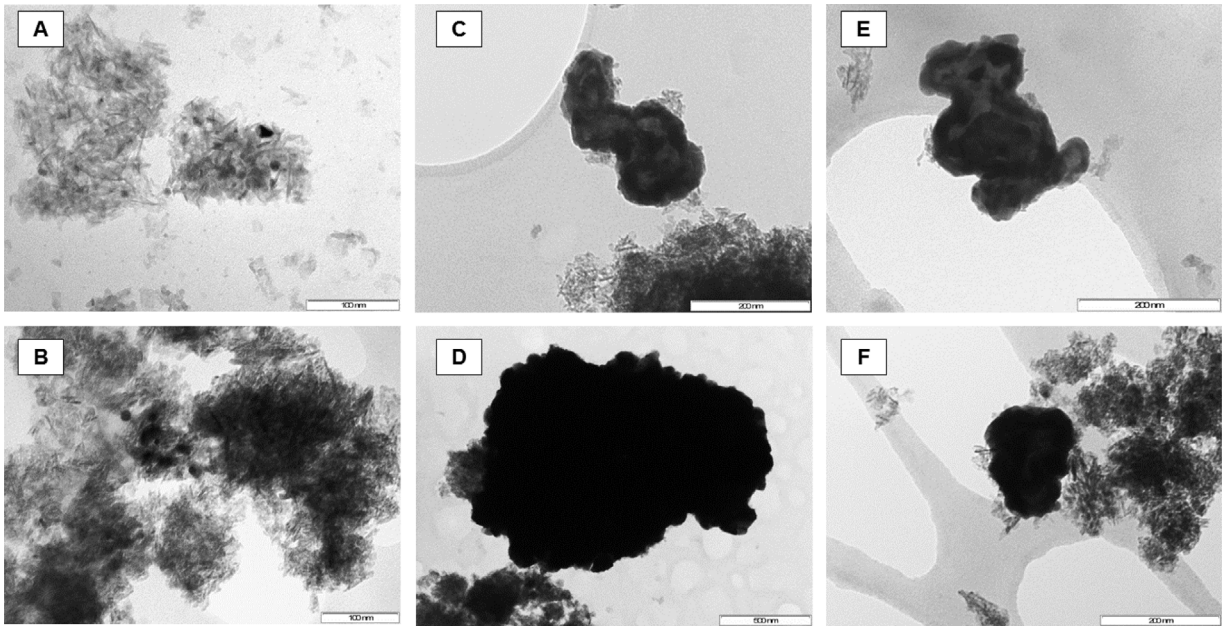

Fig. 9. Nickel particle size distribution of (A)15-NiA, (B)15-NiA-U, (C)15-NiA-P, and (D)15-NiA-H, E)15-NiA-S and (F)15-NiA-SH.

acetal selectivity shown in Figs. 4–6 supports the $AlPO_4$ formation hypothesis, which was also supported by the FTIR data (Figs. S1-S5). The experimentally observed increase in C_{24} acetal formation, is an acid catalysed process [6,34,59]. The acidity of the $AlPO_4$ phase is attributed to the P-OH groups on the surface [60], that initiate C_{24} acetal formation by protonating an octanal molecule, which then proceeds to react further with two alcohol molecules to form the acetal [6]. The reaction scheme showing the formation of octanol, and the side products formed in this study is presented in Scheme 3.

3.4. Deactivation mechanism

Evaluation of the catalytic data showed that exposure of the 15 NiA catalyst to triphenylphosphine in the feed led to a decline in the catalytic activity, which was not recovered by reintroducing clean feed into the reactor. Furthermore, the hydrogen treatment regeneration failed to recover the catalysts' activity, however, the solvent wash and combined regeneration experiment were able to recover the octanol selectivity to a significant extent when compared to the non-poisoned catalyst. Characterisation of the catalysts using ICP-OES analysis showed that phosphorus was retained after regeneration, and that the poisoned and regenerated catalysts underwent sintering, which was attributed to have been induced by phosphorus incorporation into the Ni particles.

This suggests that phosphorus not only deactivates the catalyst by poisoning, but also induces sintering of the nickel active phase, and also reacts with nickel to form a nickel phosphide phase. This phenomenon has been reported previously, where, for example, phosphorus was reported to degrade the electrochemical performance of a Ni/YSZ based half-cell during studies of solid oxide fuel cells [61,62]. This occurs via two steps. The first step involves the chemisorption of phosphorus species onto the nickel surface by coordinating with nickel, thereby 'passivating' the nickel surface [24]. The second step involves the reaction of nickel and phosphorus to form a Ni_xP_y phase, that is reportedly mobile and leads to the formation of Ni_xP_y aggregates [56,62–64].

In the present study, the reaction of nickel with phosphorus was shown to occur by magnetic measurements. The phosphorus induced migration of nickel was observed from the TEM images, which showed notable sintering of the nickel active phase. This contributed to the lower recovery of the activity and selectivity after regeneration of the

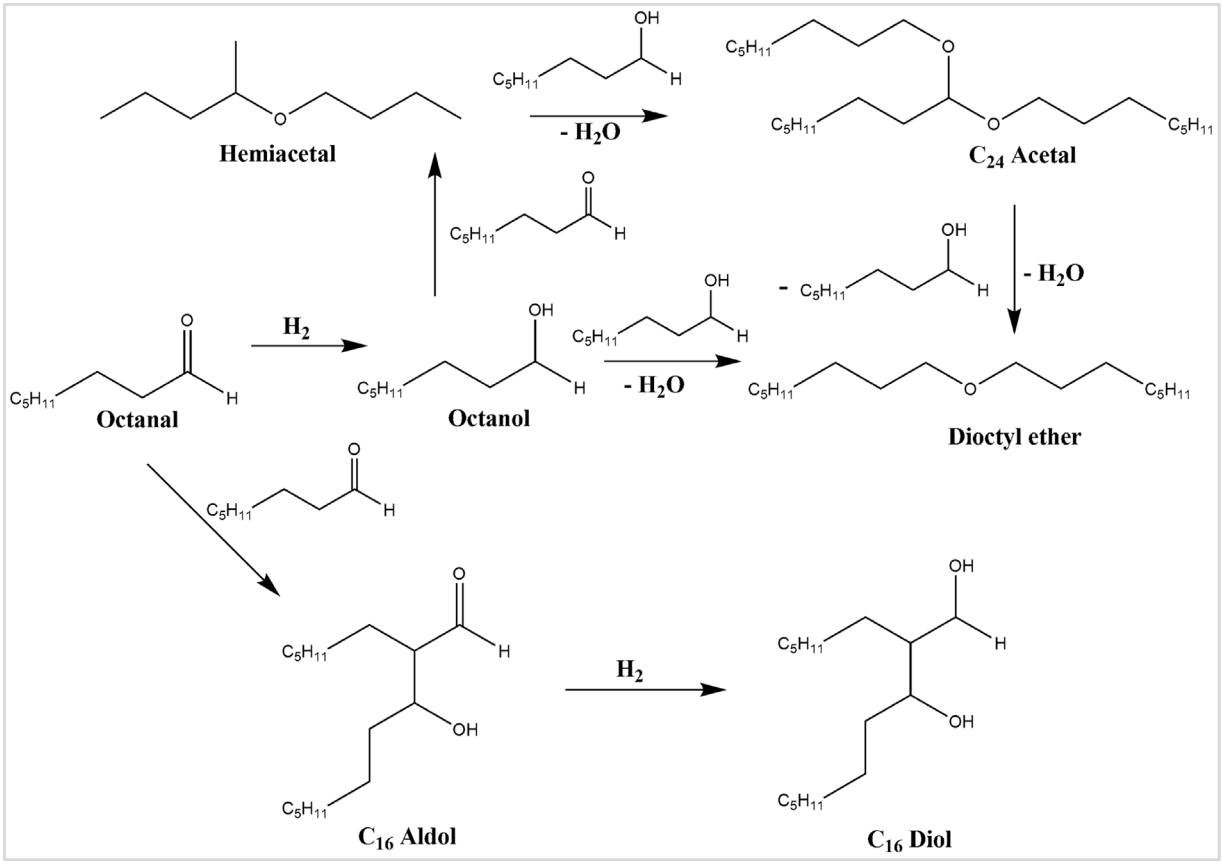

Scheme 3. Reaction scheme of octanal hydrogenation, and the accompanying side reactions catalysed by the support acid/base sites [6].

poisoned catalysts. To that effect, we postulate that exposing the catalyst to phosphorus deactivated the catalyst via a combination of phosphorus chemisorption and reaction of phosphorus with nickel to form an amorphous nickel phosphide phase. SEM-EDX line scans (Fig. S6) show a heterogeneous distribution of phosphorus on nickel for the regenerated catalysts, while hydrogen temperature programmed desorption studies showed that the non-poisoned catalyst desorbed higher quantities of hydrogen compared to 15 NiA-H and 15 NiA-SH (Table S1), suggesting that regeneration of the catalyst led to the formation of nickel phosphide phases [47].

4. Conclusions

The activity of a 15 wt.% Ni alumina supported catalyst was observed to decline with the introduction of a phosphorus poisoned feed, whereas the selectivity was not significantly affected. However, stopping the poisoned feed did not result in the recovery of the catalyst activity. In fact, it led to the loss of octanol selectivity, which was attributed to the migration of weakly bound phosphorus species from the surface of the alumina support to residual nickel active sites. Regeneration with hydrogen only, resulted in an increase in catalytic activity, however, octanol selectivity was observed to decrease after the reintroduction of clean feed. Consequentially, the C_{24} acetal selectivity increased, due to the formation of phosphorus induced, highly acidic $AlPO_4$ sites, whose presence was supported by the IR data. Regeneration with octanol washing only resulted in a slightly higher recovery of catalytic activity and more stable octanol selectivity, albeit still lower than the intrinsic selectivity. The regeneration incorporating octanol washing and hydrogen treatment showed the best recovery in both catalytic activity as well as octanol selectivity. The analyses of the used catalysts showed that the regeneration experiments did not result in the removal of phosphorus, but instead resulted in the formation of nickel phosphide phases as determined from magnetic measurements. The magnetic measurements also showed that not all of the Ni interacts with P to form Ni_xP_y phases. Thus, we were able to establish that regeneration does not remove phosphorus completely, however, phosphorus reacts with nickel to form a nickel phosphide phase, whilst also causing the migration of nickel, thereby affecting the extent to which the activity of the catalyst could be recovered with regeneration.

Acknowledgements

The authors would like to thank Sasol, the National Research Foundation of South Africa for financial support, and the Electron Microscopy Unit at the University of KwaZulu-Natal.

Appendix A. Supplementary data

Supplementary data associated with this article can be found, in the online version, at http://dx.doi.org/10.1016/j.apcatb.2017.10.064.

References

[1] G.M. Torres, R. Frauenlob, R. Franke, A. Boerner, Catal. Sci. Technol. 5 (2015) 34–54.
[2] R. Shekhar, M.A. Barteau, R.V. Plank, J.M. Vohs, J. Phys. Chem. B 101 (1997) 7939–7951.
[3] P.W.N.M. van Leeuwen, N.D. Clement, M.J.L. Tschan, Coord. Chem. Rev. 255 (2011) 1499–1517.
[4] A. Proto, R. Cucciniello, A. Genga, C. Capacchione, Catal. Commun. 68 (2015) 41–45.
[5] J.-K. Jeon, J.-H. Yim, Y.-K. Park, J. Chem. Eng. 140 (2008) 555–561.
[6] X. Wang, R.Y. Saleh, U.S. Ozkan, J. Catal. 231 (2005) 20–32.
[7] H. Liu, Q. Hu, G. Fan, L. Yang, F. Li, Catal. Sci. Technol. 5 (2015) 3960–3969.
[8] B. Chen, U. Dingerdissen, J.G.E. Krauter, H.G.J. Lansink Rotgerink, K. Moebus, D.J. Ostgard, P. Panster, T.H. Riermeier, S. Seebald, T. Tacke, H. Trauthwein, Appl. Catal. A 280 (2005) 17–46.

[9] W. Lin, H. Cheng, L. He, Y. Yu, F. Zhao, J. Catal. 303 (2013) 110–116.
[10] P. Mäki-Arvela, J. Hajek, T. Salmi, D.Y. Murzin, Appl. Catal. A 292 (2005) 1–49.
[11] X. Kong, L. Chen, Catal. Commun. 57 (2014) 45–49.
[12] J. Barrientos, M. Lualdi, M. Boutonnet, S. Jaeraas, Appl. Catal. A 486 (2014) 143–149.
[13] A.M. Amin, E. Croiset, C. Constantinou, W. Epling, Int. J. Hydrogen Energy 37 (2012) 9038–9048.
[14] C. Tanggarnjanavalukul, W. Donphai, T. Witoon, M. Chareonpanich, J. Limtrakul, J. Chem. Eng. (Amsterdam Neth.) 262 (2015) 364–371.
[15] M.D. Farahani, J. Valand, A.S. Mahomed, H.B. Friedrich, Catal. Lett. 146 (2016) 2441–2449.
[16] J.J. Birtill, Catal. Today 81 (2003) 531–545.
[17] S.T. Sie, Appl. Catal. A Gen. 212 (2001) 129–151.
[18] M.D. Argyle, C.H. Bartholomew, Catalysts 5 (2015) 145–269.
[19] P. Mäki-Arvela, G. Martin, I. Simakova, A. Tokarev, J. Warna, J. Hemming, B. Holmbom, T. Salmi, D.Y. Murzin, J. Chem. Eng. (Amsterdam Neth.) 154 (2009) 45–51.
[20] R. Quinn, T.A. Dahl, B.A. Toseland, Appl. Catal. A 272 (2004) 61–68.
[21] V. Kröger, U. Lassi, K. Kynkäänniemi, A. Suopanki, R.L. Keiski, J. Chem. Eng. 120 (2006) 113–118.
[22] M.J. Rokosz, A.E. Chen, C.K. Lowe-Ma, A.V. Kucherov, D. Benson, M.C. Paputa Peck, R.W. McCabe, Appl. Catal. B 33 (2001) 205–215.
[23] G. Westermark, H. Kariis, I. Persson, B. Liedberg, Colloids Surfs. A 150 (1999) 31–43.
[24] M. Xu, B. Li, B. Wang, X. Liu, T.S. Li, L. Chen, Electrochim. Acta 167 (2015) 147–150.
[25] J.H. Pazmino, C. Bai, J.T. Miller, F.H. Ribeiro, W.N. Delgass, Catal. Lett. 143 (2013) 1098–1107.
[26] J.R. Chang, S.L. Chang, J. Catal. 176 (1998) 42–51.
[27] J.A. Rodriguez, J. Hrbek, Acc. Chem. Res. 32 (1999) 719–728.
[28] D.C. Kim, S.S. Eom, D.H. Ko, M.H. Hong, O.H. Kwon, Method for Regenerating Hydrogenation Catalyst Poisoned During Hydrogenation of Hydroformylation Product, LG, Chem, Ltd., S. Korea, 2013 p. 18pp. Chemical Indexing Equivalent to 160:67398 (KR).
[29] M. Campanati, G. Fornasari, A. Vaccari, Catal. Today 77 (2003) 299–314.
[30] H. Xu, B.W. Zeiger, K.S. Suslick, Chem. Soc. Rev. 42 (2013) 2555–2567.
[31] D. Peters, J. Mater. Chem. 6 (1996) 1605–1618.
[32] A. Bazyari, Y. Mortazavi, A.A. Khodadadi, L.T. Thompson, R. Tafreshi, A. Zaker, O.T. Ajenifujah, Appl. Catal. B 180 (2016) 312–323.
[33] V.D.B.C. Dasireddy, S. Singh, H.B. Friedrich, Appl. Catal. A 421–422 (2012) 58–69.
[34] T. Chetty, H.B. Friedrich, V.D.B.C. Dasireddy, A. Govender, P.J. Mohlala, W. Barnard, ChemCatChem 6 (2014) 2384–2393.
[35] G. Zhu, C. Xi, H. Xu, D. Zheng, Y. Liu, X. Xu, X. Shen, RSC Adv. 2 (2012) 4236–4241.
[36] S.R. Yenumala, S.K. Maity, D. Shee, Catal. Sci. Technol. 6 (2016) 3156–3165.
[37] D.R. Abd El-Hafiz, M.A. Ebiad, R.A. El-salamony, Mater. Renew. Sustain. Energy 3 (2014) 1–13.
[38] J. Valand, A.S. Mahomed, S. Singh, H.B. Friedrich, J. Porous Mater. 23 (2016) 175–183.
[39] A.J. McCue, F.-M. McKenna, J.A. Anderson, Catal. Sci. Technol. 5 (2015) 2449–2459.
[40] H.P. Buwono, S. Minami, K. Uemura, M. Machida, Ind. Eng. Chem. Res. 54 (2015) 7233–7240.
[41] G. Westermark, I. Persson, Colloids Surf. A 144 (1998) 149–166.
[42] P. Forzatti, L. Lietti, Catal. Today 52 (1999) 165–181.
[43] S. Carenco, X.F. Le Goff, J. Shi, L. Roiban, O. Ersen, C. Boissiere, C. Sanchez, N. Mezailles, Chem. Mater. 23 (2011) 2270–2277.
[44] H. Guo, G. Iqbal, B.S. Kang, Int. J. Appl. Ceram. Technol. 8 (2011) 68–73.
[45] H. Kishimoto, K. Yamaji, M.E. Brito, T. Horita, H. Yokokawa, J. Min. Metall. Sect. B 44 (2008) 39–48.
[46] R.-K. Chiang, R.-T. Chiang, Inorg. Chem. 46 (2007) 369–371.
[47] Y. Tan, D. Sun, H. Yu, B. Yang, Y. Gong, S. Yan, Z. Chen, Q. Cai, Z. Wu, CrystEngComm 16 (2014) 9657–9668.
[48] T. Watanabe, J. Kato, S. Matsuo, H. Wakita, N. Umesaki, X-ray Spectrom. 30 (2001) 15–20.
[49] J. Chen, L. Sun, R. Wang, J. Zhang, Catal. Lett. 133 (2009) 346–353.
[50] R.B. Wexler, J.M.P. Martirez, A.M. Rappe, Chem. Mater. 28 (2016) 5365–5372.
[51] X. Li, H. Cheng, G. Liang, L. He, W. Lin, Y. Yu, F. Zhao, Catalysts 5 (2015) 759–773.
[52] S.J. Sawhill, K.A. Layman, D.R. Van Wyk, M.H. Engelhard, C. Wang, M.E. Bussell, J. Catal. 231 (2005) 300–313.
[53] R. Chakrabarti, S.A. Tupy, L.D. Schmidt, Energy Fuels 25 (2011) 4763–4769.
[54] J. Chen, M. Han, S. Zhao, Z. Pan, Z. Zhang, Catal. Sci. Technol. 6 (2016) 3938–3949.
[55] L.M. Moreau, D.-H. Ha, H. Zhang, R. Hovden, D.A. Muller, R.D. Robinson, Chem. Mater. 25 (2013) 2394–2403.
[56] H. Sezer, I.B. Celik, Electrochim. Acta 155 (2015) 421–430.
[57] J. Chen, S. Zhou, D. Ci, J. Zhang, R. Wang, J. Zhang, Ind. Eng. Chem. Res. 48 (2009) 3812–3819.
[58] E.C. DeCanio, J.C. Edwards, T.R. Scalzo, D.A. Storm, J.W. Bruno, J. Catal. 132 (1991) 498–511.
[59] J.M. Bell, D.G. Kubler, P. Sartwell, R.G. Zepp, J. O. C. 30 (1965) 4284–4292.
[60] M. Machida, S. Minami, K. Ikeue, S. Hinokuma, Y. Nagao, T. Sato, Y. Nakahara, Chem. Mater. 26 (2014) 5799–5805.
[61] O. Demircan, W. Zhang, C. Xu, J. Zondlo, H.O. Finklea, J. Power Sources 195 (2010) 3091–3096.
[62] C. Xu, J.W. Zondlo, H.O. Finklea, O. Demircan, M. Gong, X.B. Liu, J. Power Sources 193 (2009) 739–746.
[63] Y. Chen, S. Chen, G. Hackett, H. Finklea, J. Zondlo, I. Celik, X. Song, K. Gerdes, Solid State Ionics 234 (2013) 25–32.
[64] K. Haga, Y. Shiratori, Y. Nojiri, K. Ito, K. Sasaki, J. Electrochem. Soc. 157 (2010) B1693–B1700.